Numerical and Experimental Analysis of Self-Protection in Reinforced Concrete due to Application of Mg–Al–NO$_2$ Layered Double Hydroxides

Zahid Mohammad Mir,* Alexandre Bastos, Celestino Gomes, Urs Mueller, Maria Cruz Alonso, Kristina Villar, Miguel P. Rabade, Frederico Maia, Cláudia M. Rocha, Philippe Mainçon, Daniel Höche, Mario G. S. Ferreira, and Mikhail L. Zheludkevich

Concrete possesses an intrinsic chloride binding capacity. Chloride ions from the environment bind with the hydrated cementitious phases in the form of bound chlorides. The contribution of chemically bound chlorides toward increasing the service life of concrete structures is vital as they help in slowing down the chloride diffusion in the concrete thereby delaying reinforcement depassivation. The authors attempt to increase the chloride binding capacity of concrete by adding a small amount of Mg–Al–NO$_2$ layered double hydroxides (LDHs) with the objective to delay reinforcement corrosion and by this to considerably extend the service life of concrete structures situated in harsh environments. This study presents numerical and experimental analysis of the action of LDH in concrete. Formation factor is used to determine the effective chloride diffusion coefficient. In addition, the chloride binding isotherms together with Poisson–Nernst–Planck equations are used to model the chloride ingress. A comparable chloride binding is observed for concrete with and without Mg–Al–NO$_2$, depicting only a slight chloride uptake by Mg–Al–NO$_2$. Further investigations are conducted to understand this behavior by studying the stability and chloride entrapping capacity Mg–Al–NO$_2$ in concrete.

1. Introduction

Concrete structures are prone to reinforcement corrosion induced damage due to chloride ingress.[1,2] Chloride ingress occurs in infrastructures exposed to the marine environment (offshore or costal structures), or due to the action of deicing salts in structures along roadways.[3] Concrete damage due to reinforcement corrosion is the most common factor for repair and maintenance of concrete structures. This problem has global economic and social consequences with huge associated investments and strong impact on society due to closing of roads for the repair of bridges, tunnels, and bottlenecks in the water and energy production and distribution.[4]

The alkaline environment of concrete protects the reinforcement by forming a passive layer around the rebar.[5] As concrete is exposed to chloride ions during its service life, these ions pass through the concrete cover and in due course of time reach the

Z. M. Mir, Dr. D. Höche, Prof. M. L. Zheludkevich
Surface and Coating Technology
Institute of Materials Research
Helmholtz-Zentrum Geesthacht Centre for Materials and Coastal Research
Max-Planck Str. 1, 21502 Geesthacht, Germany
E-mail: zahid.mir@hzg.de

Dr. A. Bastos, C. Gomes, Prof. M. G. S. Ferreira
DEMaC – Department of Materials and Ceramic Engineering
CICECO – Aveiro Institute of Materials
Universidade de Aveiro
3810-193 Aveiro, Portugal

The ORCID identification number(s) for the author(s) of this article can be found under https://doi.org/10.1002/adem.202000398.

Dr. U. Mueller, Dr. M. P. Rabade
Infrastructure and Concrete Technology
RISE Research Institutes of Sweden
Brinellgatan 4, 504 62 Borås, Sweden

Dr. M. C. Alonso, K. Villar
CSIC
Institute of Construction Science Eduardo Torroja
Serrano Galvache, 4, 28033 Madrid, Spain

Dr. F. Maia, Dr. C. M. Rocha
SmallMaTek LDA
Rua dos Canhas, 3810-075 Aveiro, Portugal

Dr. P. Mainçon
SINTEF Materials and Chemistry
7465 Trondheim, Norway

Prof. M. L. Zheludkevich
Faculty of Engineering
University of Kiel
Kaiserstrasse 2, 24143 Kiel, Germany

rebar surface.[6] Chloride concentrations above a certain threshold can damage the passive layer and initiate corrosion on the rebar surface.[7] Continuation of this process leads to accumulation of corrosion products at the steel–concrete interface (SCI).[8] Corrosion products are less denser than parent steel and therefore exhibit a higher volume.[2,9] Due to the limitation of space at the SCI, the accumulation of corrosion products leads to an increase in the interface pressure resulting in microcracking of the concrete around the rebar.[10,11] As the process continues, these microcracks coalesce to form macrocracks[12,13] which can potentially lead to spalling of the concrete cover and eventually turn the structure nonoperational or in need of repair.

Chloride ions enter the concrete via the pore system filled with pore solution in the saturated state.[14] Most of the pore system consists of interstices formed by the nano- and microsized crystals and lamellas of the hydrate phases (C–S–H, AFm, AFt, CH, and so on[15]). Only a smaller amount of porosity consists of air voids or larger capillary pores. Chloride ions therefore transport themselves in the pore solution (free chlorides) and interact with the cementitious microstructure surrounding the pore system. This interaction can lead to chemical and physical binding of chloride ions with hydration products (bound chlorides).[16,17] The total chloride content in concrete is therefore a combination of free and bound chlorides. The binding of chlorides slows the ingress of free chlorides along the pore network. Therefore, an accurate determination of chloride binding is necessary to create precise service life estimation models.

There are many ways by which the concrete's ability to bind chlorides can be increased. The addition of supplementary cementitious materials such as fly ash, ground granulated blast furnace slag, and metakaolin has been reported to increase the binding capacity in concrete.[18] In the LORCENIS project,[19] novel chloride entrapping nanocontainers were developed with an aim to impart additional chloride binding capabilities to concrete. In this study, one of the recently developed nanocontainers of Mg–Al–NO_2 layered double hydroxides (LDHs) are used as chloride binding additives inside concrete.

LDHs are finely powdered materials which can be easily added to concrete during the mixing process. LDH can be prepared by the coprecipitation method[20] of two different metallic hydroxides, in our case Mg and Al. As a result of coprecipitation,

bimetallic hydroxides are formed with a layered structure, hence the name LDHs. These hydroxide layers are composed of positively charged cations with anions in between the layers (galleries) to balance the charge (**Figure 1**). LDH possesses a unique ability, in the sense that they can intercalate an external anion from the environment, e.g., a Cl^- ion, by exchanging it with an originally intercalated anion, e.g., a corrosion inhibiting ion.[21] This property is termed as the ionic exchange property of LDH.[22] With this application in mind, LDH is a potential candidate to release anions from its interlayers which can be a corrosion inhibiting ion/species and can also provide additional chloride capture in concrete. Concrete mixed with LDH could show improved chloride binding capability and controlled corrosion inhibitor release. This property has been termed as "self-protection" of reinforced concrete in the LORCENIS project. This work only focuses on the chloride capture capability and not on the inhibitor release from LDH.

In the recent years, many studies have focused on the use of LDH in concrete. Cao et al.[23] used Mg-based LDH in chloride solutions and observed a decrease in the chloride ion concentration with time. Zuo et al.[24] conducted studies related to the chloride ion capture capacity by Mg-based LDH and reported considerable chloride loading in aqueous solutions following a Langmuir-type isotherm. Yang et al.[25] used Mg–Al LDH into cement pastes and mortars and found that an appropriate addition increased the time to corrosion. X-ray diffraction (XRD) analysis and thermogravimetric analysis (TGA) studies by Yang et al.[26] focused on chloride uptake by Ca–Al-based LDH in chloride solutions. They demonstrated a considerable chloride uptake by Ca-based LDH. The effect of addition of LDH in cement paste on the setting, hydration, as well as microstructure development was investigated by Wu et al.[27]

In this study, we investigated the use of LDH for additional chloride capture in concrete. Two concrete recipes, one control (without LDH) and another one with 2% LDH (with respect to cement content and 0.3% of overall concrete), were compared and results were gained experimentally as well as by modeling. To accurately model the chloride ingress, mostly two major input parameters are required, i.e., microstructural information and chloride binding capacity isotherms. An accurate estimation of
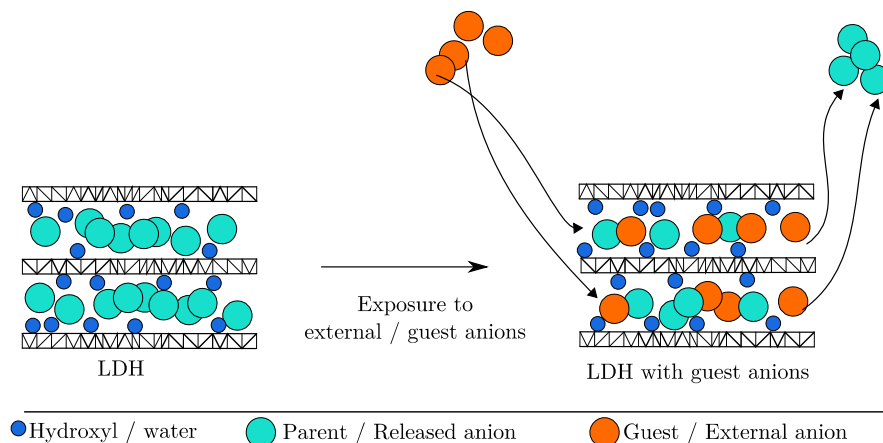

Figure 1. A schematic representation of the ionic exchange property of LDHs.

- ● Hydroxyl / water
- ● Parent / Released anion
- ● Guest / External anion

microstructure in terms of diffusion coefficient can aid in the modeling of transport of free chlorides.

The formation factor ($\mathcal{FF}_c$) was used to quantify the effect of microstructure on the ionic transport.[28,29] $\mathcal{FF}_c$ has been regarded as a fundamental measure toward microstructural characterization of porous media. Due to the ease with which $\mathcal{FF}_c$ can be obtained, it is possible to quickly obtain transport properties of various concrete recipes in a rapid and reliable way. Together with $\mathcal{FF}_c$, the second vital parameter for service life modeling is the chloride binding capacity. Freundlich-type isotherm was used due to its good fit with our experiments.[30] These inputs were derived for both types of concretes, i.e., control (REF) and with 2% LDH (+2% LDH).

Chloride transport was modeled in water-saturated concrete using the Nernst–Planck equation and combines information from $\mathcal{FF}_c$ and chloride binding isotherms.[31] The transport of charged ions through the pore network gives rise to a potential field which is accounted via the Poisson's equation.[32] The resulting coupled system of equations was solved using the finite element method[33] for a 1D domain. The numerical model was used to compare the chloride transport in the concrete with and without LDH. Experimental verification of simulation results is also presented. In addition, the article highlights the stability of LDH in cementitious environments to explain the reduced chloride uptake by Mg–Al–NO_2 in the cementitious matrix.

2. Materials

2.1. Synthesis of LDH

The LDH used in this study was provided by Smallmatek, Lda (Portugal) and prepared according to their own production procedures. Briefly, the Mg/Al–NO_2 LDH was prepared by coprecipitation of Mg and Al salts in a solution with excess of sodium nitrite, where the pH range was adjusted with sodium hydroxide (Poznyak et al.[34]). The production process was conducted in a custom-made pilot-scale reactor equipped with a proportional–integral–derivative (PID) controller, which allows the control and correction of important process parameters (i.e., pH and temperature), and peristaltic pumps for precise addition of chemicals. Finally, the obtained slurry was washed with deionized water and filtered under reduced pressure, then dried using an industrial spray dryer to guarantee uniform fine powders.

2.2. Concrete Mix Description

Two series of concrete specimens were prepared: the reference concrete (REF) without and with 2% LDH (+2% LDH). The respective mix details are shown in **Table 1**. The cement was supplied by Dyckerhoff (Germany) and the specimens were cast at Research Institutes of Sweden (RISE, Sweden). Tests were conducted jointly at RISE, Spanish National Research Council (CSIC, Spain), University of Aveiro (Portugal), and Helmholtz-Zentrum Geesthacht (HZG, Germany). In addition, cement paste specimen were cast with the CEM I 42.5 LA SR consisting of low calcium aluminate content having 0.5 water cement ratio (w/c) and 2%-4% LDH content for investigating the stability of LDH in cement pastes, as explained later in Section 4.

Table 1. Concrete composition for REF and +2% LDH mixes. Chemical and mineralogical composition of binder is also included.

Property [unit]	REF	+2% LDH
Cement CEM I/52.5 R [kg m^{-3}]	350	350
LDH [mass% binder] [mass% total mass]	0	2 (0.3)
Aggregate 0–4 mm [kg m^{-3}]	1151	1151
Aggregate 4–8 mm [kg m^{-3}]	265	265
Aggregate 8–16 mm [kg m^{-3}]	355	355
Super plasticizer [mass% binder]	0.8	0.8
Water/cement ratio [1]	0.6	0.6
Chemical composition (binder)		
SiO_2 [%]	–	21.39
Al_2O_3 [%]	–	3.69
Fe_2O_3 [%]	–	1.29
CaO [%]	–	64.66
MgO [%]	–	0.72
SO_3 [%]	–	3.43
K_2O [%]	–	0.57
Na_2O [%]	–	0.21
Mineralogical composition (binder)		
C_3S [%]	–	70.3
C_2S [%]	–	6.5
C_3A [%]	–	8.9
C_4AF [%]	–	2.4
Calcite [%]	–	4.7
Gypsum [%]	–	3.7
Others [%]	–	3.6

3. Numerical Model

3.1. Application of Formation Factor for Microstructure Characterization

The exact determination of diffusion coefficients of chloride ions in the concrete pore solution $\mathcal{D}_{cl}^p$ is a difficult parameter to obtain, due to ionic interactions, heterogeneity of concrete, and variability of samples, and can lead to deviations. In contrast, the diffusion coefficient of chloride ions at infinite dilution in a volume of liquid $\mathcal{D}_{cl}^\infty$ is well established ($\mathcal{D}_{cl}^\infty = 2.030 \times 10^{-9}$ m^2 s^{-1}). The diffusion of chloride ion in a single linear pore without any other interactions can be obtained using the $\mathcal{D}_{cl}^p$. When up-scaling the transport parameter from a single pore to a representative volume element (RVE) of concrete, the porous microstructure in the RVE can be accounted using an effective diffusion coefficient $\mathcal{D}_{cl}^{eff}$.[35] It also does not include any ion–ion or ion–solid interactions and accounts only for the hindrance offered by the porous microstructure of the RVE. $\mathcal{D}_{cl}^{eff}$ is sometimes also referred to by other authors as the microstructural diffusion coefficient.[29]

The ion–ion and ion–solid interactions may then well be considered using the apparent diffusion coefficient or bulk diffusion coefficient $\mathcal{D}_{cl}^{app}$. $\mathcal{D}_{cl}^{app}$ is commonly used in many service-life

models but it does not distinguish microstructural corrections and chloride binding effects. It is of vital importance to separate the effects of microstructure and ionic interactions to deeply understand the chloride transport in a concrete mix and in our case the effect of LDH. As complex as it may sound, these two properties can be separated by a material property known as the formation factor ($\mathcal{FF}_c$).

$\mathcal{FF}_c$ simply uses the electrical properties of a medium to quantify the microstructure, independently of the chemistry of the conducting fluid. The concept was originally used by Archie in geological research.[36] The formation factor can be defined as the ratio of pore solution conductivity to the bulk conductivity of a saturated porous material. It can be expressed as

$$\mathcal{FF}_c = \frac{\sigma_p}{\sigma_b} \tag{1}$$

where σ_p is the pore solution conductivity (S m^{-1}) and σ_b is the bulk solution conductivity (S m^{-1}), which includes the effect of porosity.

The overall conductivity of an electrolyte is directly proportional to the mobility of each ion in the solution. According to the Einstein's mobility equation, the mobility of an ion is directly proportional to the diffusion coefficient of the ion.[29,37] Therefore

$$\sigma \propto \mathcal{U}_i^m \propto \mathcal{D}_i \tag{2}$$

where $\mathcal{U}_i^m$ is the ionic mobility and $\mathcal{D}_i$ is the diffusivity of the ion.

Using Equation (2), $\mathcal{FF}_c$ can be further expressed as

$$\mathcal{FF}_c = \frac{\mathcal{D}_{cl}^{\infty}}{\mathcal{D}_{cl}^{eff}} \tag{3}$$

As such, $\mathcal{FF}_c$ is a fundamental material parameter which sets up a direct relation between the $\mathcal{D}_{cl}^{\infty}$ and the effective diffusion coefficient $\mathcal{D}_{cl}^{eff}$ of a porous nonconducting material filled with a conducting liquid. For a detailed underlying mathematical and physical understanding, the reader is directed to the works of Weiss et al.[28] and Snyder.[29] Chloride diffusion tests usually take months or years to complete and $\mathcal{FF}_c$ can be obtained very fast by setting up simple conductivity experiments in the lab and applying Equation (1).

Once $\mathcal{FF}_c$ is known, $\mathcal{D}_{cl}^{eff}$ can be expressed as function of $\mathcal{FF}_c$ and $\mathcal{D}_{cl}^{\infty}$

$$\mathcal{D}_{cl}^{eff} = \frac{\mathcal{D}_{cl}^{\infty}}{\mathcal{FF}_c} \tag{4}$$

$\mathcal{FF}_c$ is a nondimensional parameter and independent of ionic interactions, and it does not consider chloride binding. There are four major benefits of this approach: 1) Once $\mathcal{FF}_c$ is evaluated, the effective diffusivity of any ion in a porous medium can be easily obtained. 2) The biggest advantage of using $\mathcal{FF}_c$ lies in service life models where effective diffusion coefficients are required for chloride ion transport and as such service life models can be set up easily and accurately. This is discussed later in more detail. 3) Microstructure and transport properties of many different concrete mix/recipes can be quickly compared in terms of durability requirements.

4) As $\mathcal{FF}_c$ is independent of the ion–ion and ion–solid interactions, one can separately account for the chloride binding effects. The biggest benefit comes from the fact that using $\mathcal{FF}_c$ it is possible to not only quantify the microstructure but also separate ion binding effect of the ion from the transport phase. Therefore, the chloride binding can be evaluated separately using suitable data of isotherms[17,38] and can be easily added to the transport equations.

The significance of using $\mathcal{FF}_c$ in this study is that a direct influence of the addition of 2% LDH on the porous network can be acquired, to obtain the effective diffusion coefficients and also account for separately the chloride binding of hydrate phases as well as LDH in the transport model. This is explained in the later sections.

3.2. 1D Transport Model

The transport of an ion in a single saturated confined pore may be expressed using Nernst–Planck transport equation as[32]

$$\frac{\partial}{\partial t}\left(\mathcal{C}_i^{\dagger}\right) + \nabla \cdot \left(-\mathcal{D}_i^p\left(\nabla \mathcal{C}_i^{\dagger} + \mathcal{C}_i^{\dagger}\frac{z_i\mathcal{F}}{\mathcal{R}\mathcal{T}}\nabla\psi_e + \mathcal{C}_i^{\dagger}\nabla(\ln\Upsilon_i)\right)\right) = 0 \tag{5}$$

where $\mathcal{C}_i^{\dagger}$ is the free ion concentration (in mol m^{-3}) in the pore solution, $\mathcal{D}_i^p$ is the diffusion coefficient of the ion in pore solution (in m^2 s^{-1}), z_i is the charge number, $\mathcal{F}$ is the Faraday's constant (96 485 C mol^{-1}), $\mathcal{R}$ is the ideal gas constant (8.314 J mol^{-1} K^{-1}), $\mathcal{T}$ is temperature (293 K), ψ_e is the electric potential (V) in the electrolyte, and Υ_i is the chemical activity coefficient.

To account for the porous network, Equation (5) can be alternatively written for a RVE of concrete using the formation factor as described in Qiao et al.[31]

$$\begin{aligned}\theta_p\frac{\partial}{\partial t}\left(\mathcal{C}_i^{\dagger}\right) \\ + \nabla \cdot \left(-\frac{\mathcal{D}_i^{\infty}}{\mathcal{FF}_c}\left(\nabla \mathcal{C}_i^{\dagger} + \mathcal{C}_i^{\dagger}\frac{z_i\mathcal{F}}{\mathcal{R}\mathcal{T}}\nabla\psi_e + \mathcal{C}_i^{\dagger}\nabla(\ln\Upsilon_i)\right)\right) = 0\end{aligned} \tag{6}$$

where θ_p is the porosity of the RVE.

Equation (6) expresses the transport of ionic species considering the effect of the concrete microstructure in a completely saturated state. To include the amount of chlorides that may bind to the cementitious microstructure, a source/sink term can be introduced in Equation (6). The resulting equation can be expressed as

$$\begin{aligned}\theta_p\frac{\partial}{\partial t}\left(\mathcal{C}_i^{\dagger}\right) + \frac{\partial}{\partial t}\left(\mathcal{C}_i^{b}\right) \\ + \nabla \cdot \left(-\frac{\mathcal{D}_i^{\infty}}{\mathcal{FF}_c}\left(\nabla \mathcal{C}_i^{\dagger} + \mathcal{C}_i^{\dagger}\frac{z_i\mathcal{F}}{\mathcal{R}\mathcal{T}}\nabla\psi_e + \mathcal{C}_i^{\dagger}\nabla(\ln\Upsilon_i)\right)\right) = 0\end{aligned} \tag{7}$$

with $\mathcal{C}_i^{b} = 0 \ \forall i \neq Cl^{-}$ \tag{8}

where $\mathcal{C}_i^{b}$ is the amount of bound ions (mol m^{-3} of concrete).

Equation (7) includes diffusive flux, migration flux, and ion interactions taking place in ionic solution due to chemical activity effects. As we are mostly interested in chloride binding, the binding term for other species is equated to zero as described in

Equation (8). The bound chlorides can be specifically expressed as a function of free chlorides, determined usually by fitting an Freundlich-type isotherm to the experimental data points as

$$C_{Cl^-}^t = f\left(C_{Cl^-}^{\dagger}\right) = a\left(C_{Cl^-}^{\dagger}\right)^b \tag{9}$$

where a and b are Freundlich isotherm parameters.[38]

The experimental procedure for obtaining the chloride binding isotherm is explained later. The total chloride in concrete may then be expresses as

$$C_{Cl^-}^t = \theta_p C_{Cl^-}^{\dagger} + C_{Cl^-}^b \tag{10}$$

where $C_{Cl^-}^t$ is expressed as $\mathrm{mol\,m^{-3}}$ of concrete.

The concrete pore solution is composed of different ions and the velocity with which ions move in the solution is different. In this study, six commonly present[32] ionic species are taken into account namely Cl^-, K^+, OH^-, Na^+, Ca^{2+}, and SO_4^{2-}. In addition, one solid phase in the form of bound chloride is also accounted. This phase is assumed to be electrically neutral. Al^{3+} and NO_2^- were also detected in the pore solution but were not included to keep the model computationally inexpensive. However, the role of these species is explained later in the stability studies.

In a diluted state, different ionic species move at different velocity and as such some charged species move faster than others. This creates an electric field between the species which slows down fast moving ions and subsequently accelerates slow moving ions to maintain an electrically neutral environment. As such, a gradient of potential is created which is responsible for the migration flux in the diluted medium.

This electric field ψ_e, can be expressed as function of concentration of species and their respective charge via Poisson's equation as[39,40]

$$\nabla^2 \psi_e = -\frac{\mathcal{F}}{\mathcal{E}_o \mathcal{E}_r}\left(\sum_{i=1}^{i^t} C_i z_i\right) \tag{11}$$

where $\mathcal{E}_o$ is the permittivity of the vacuum and $\mathcal{E}_r$ is the relative permittivity of water.[40] The index i^t includes all ionic species and i^t is the total number of species.

The electrostatic interactions between opposite and like charged species also affect the movement of ions. At low solute concentrations, chemical activity effects are almost negligible. However, at higher concentrations, these effects can considerably affect the transport of ions. These interactions can be accounted using the modified Davies equations as reported by Samson et al.[32,41]

$$\ln \Upsilon_i = \mathcal{A}_z i^2 I_m \left(\frac{-I_m^{-0.5}}{1 + a_i \mathcal{B} I_m^{0.5}} + \frac{(0.2 - 4.17 \times 10^{-5} I_m)}{\sqrt{1000}}\right) \tag{12}$$

where $\mathcal{A}$ and $\mathcal{B}$ are temperature-dependent parameters, I_m is the ionic strength and a_i being the respective diameters of each ion. The detailed expressions and given values of some species are mentioned in ref.[41] and **Table 2**.

Chloride transport can be modeled as a 1D problem for concrete samples exposed to chlorides only along one planer surface. A simplified 1D domain, 100 mm in length, was set up and meshed with linear elements. A finer mesh (0.25–0.5 mm element size) was used for the first 5 mm of the domain to handle steep concentration gradients and the rest was meshed with a relatively coarse mesh (1 mm element size) as shown in **Figure 2**. The aforementioned system of equations was solved using finite element method[33] in COMSOL Multiphysics software package. Only strong forms of the equations are presented for the sake of brevity and conciseness. Quadratic Lagrange shape functions were used and the resulting system of equations was solved using an implicit time integration scheme, as implicit time marching is unconditionally stable.

To compare the two mixes, i.e., REF and +2% LDH, the model simulates a standard ponding test for both the mixes. As such one end of the geometry at $x = 0$ (mm) is exposed to a NaCl concentration of $165\,\mathrm{g\,L^{-1}}$ ($2823\,\mathrm{mol\,m^{-3}}$).[31,42] The details of

Table 2. Diffusion coefficient at infinite dilution and ionic radii as per refs. [39,54].

Species	$\mathcal{D}_i^{\infty}$ [m² s⁻¹]	a_i [Å]
Cl^-	2.030×10^{-9}	3
K^+	1.960×10^{-9}	3
OH^-	5.270×10^{-9}	3.5
Na^+	1.330×10^{-9}	4
Ca^{2+}	0.793×10^{-9}	6
SO_4^{2-}	1.070×10^{-9}	6

x = 0 (Dirichlet B.C.)

95 mm (Coarse mesh)
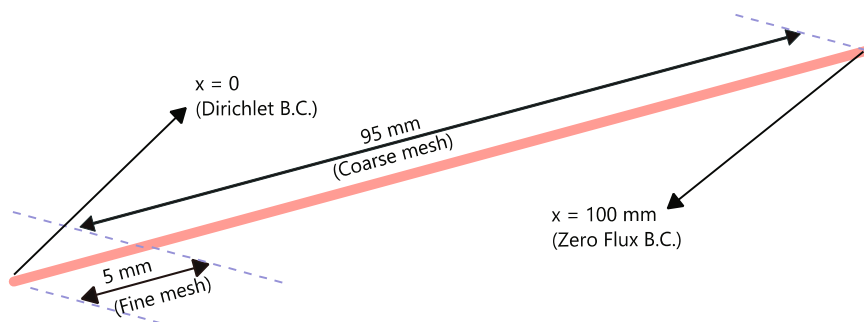
x = 100 mm (Zero Flux B.C.)

5 mm (Fine mesh)

Figure 2. 1D modeling domain. Exposure end at ($x = 0$ mm; B.C. stands for boundary conditions).

the ponding test as well as the initial conditions for both the mixes are described in Section 4.

4. Experimental Section

4.1. Experimental Determination of Formation Factor

The formation factor was calculated by measuring the resistivity of lime saturated concrete samples at 28 days of age and from resistivity of pore solutions obtained from cement pastes at 7 days of age. The respective mix details are shown in Table 1.

During the curing period, the electrical resistance evolution was measured weekly. The samples were saturated under vacuum, by applying vacuum for 3 h and then adding saturated lime. When the samples were completely covered, the vacuum pump was left running for additional 1 h. The electrical resistivity was determined through the impedance measured with an FRA module applying an AC current of a frequency of 1000 Hz based on standard for determination of electrical resistivity.[43] The samples were in contact with two stainless steel meshes used as electrodes connected to the equipment. Two sponges were moistened using limewater to improve the contact of the sample with the electrodes. The electrical resistance of the sponges was also measured to remove its value from the calculation. The measured values of conductivity are shown in **Table 3**.

The electrical resistivity of the pore solution was measured in cement paste samples after 7 days of curing. To determine this, the pore fluid of the cement paste was extracted by the pore pressing method. The procedure from Alonso et al. was followed.[44] Approximately 125 g of the sample was placed into the cavity of the pore pressing apparatus. Pressure is then applied to a piston according to a maximum pressure of 400–500 MPa up to 650 MPa. Pressure is increased gradually with a mean rate of 50 MPa min^{-1}. The pore fluid is collected in a syringe, which was connected to the hole of the bottom plate via a short flexible plastic tube. After collection, the pore fluid was immediately filtered through a 0.45 μm filter and stored in a sealed plastic container protected from atmospheric CO_2 until further analysis. Two pore pressing tests were made for each cement paste type, i.e., with and without LDH. Immediately after collecting the pore solution, the electrical conductivity and pH of this aqueous solution was measured and is shown in Table 3. Further analyses were conducted to measure the ionic content of the pore fluids using inductively coupled plasma optical emission spectrometry (ICP-OES) and ionic chromatography (IC) (Table 4).

4.2. Chloride Binding Capacity

The chloride binding was evaluated by exposing ground cement pastes to various chloride solutions as in previous works.[17,38,45] Two cement pastes with 2% LDH and without LDH were prepared with deionized water with w/c of 0.5 instead of 0.6[46] to avoid cement bleeding. The pastes were cast in cylindrical airtight containers and rotated at slow speed within the first 24 h to prevent any segregation. After 28 days of curing, the samples were ground to a fine powder and dried at room temperature in a sealed lab desiccator with silica gel. 10 g of each powder was then exposed to 50 mL solutions of seven different chloride concentrations: 0.1, 0.3, 0.5, 0.7, 1.0, 2.0, and 3.0 M, respectively, for 7 days in sealed containers. The samples were stirred using a magnetic stirrer each day for 1 h. All samples were kept airtight during the experimental process to reduce the risk of carbonation. After 7 days, the free chloride concentration in the samples was measured by performing potentiometric measurement using a Mettler Toledo S7 Excellence together with a chloride sensitive electrode (Mettler Toledo Dx-235 Cl sensitive sensor). As a result of physical and chemical chloride binding, the concentration of chloride ion in the solution decreases. The total bound chlorides can be calculated by measuring the decrease in chloride concentration in the test solution. After 7 days, it is assumed that an equilibrium is established between the bound and free chlorides and the solution characteristics match the pore solution characteristics.

A plot between the final equilibrium chloride concentration ($C_{Cl^-}^{Eq.}$) and the amount of bound chlorides ($C_{Cl^-}^{b}$) results fitted to a Freundlich isotherm, as shown in Equation (9) and is the so-called chloride binding isotherm. **Table 5** shows the fitted parameters for a Freundlich isotherm for each mix.

4.3. Porosity, Density, and Ponding Test

The water-accessible porosity and saturated density tests were conducted according to UNE 83980[47] after 28 days of age of

Table 3. Experimentally measured input parameters for REF and +2% LDH. Conductivity values are presented instead of resistivity. ϱ_{con} refers to the density of concrete.

Parameter	REF	+2% LDH
σ_p [S m^{-1}]	7.238	7.36
σ_b [S m^{-1}]	0.0242	0.02
$\mathcal{FF}_c$	298.9	368
θ_p [%]	11.6	12.1
ϱ_{con} [kg m^{-3}]	2340	2340

Table 4. Initial concentration measured experimentally from pore solution. These concentrations are used as initial conditions in the FEM model excluding Al^{3+} and NO_2^-. All concentration are expressed in mol m^{-3}.

Mix	Species included in the model						Species not included	
	Cl^-	K^+	OH^-/(pH)	Na^+	Ca^{2+}	SO_4^{2-}	Al^{3+}	NO_2^-
REF	1.86	275.27	285.10/(13.45)	140.57	0.41	1.276	0.042	–
+2% LDH	2.805	282.73	239.88/(13.38)	179.54	0.188	1.61	0.0415	37.25

Table 5. Freundlich isotherm parameters for REF and +2% LDH mixes.

Property	REF	+2% LDH
a	5.7037	5.4898
b	0.4617	0.4749
Fitted R^2	0.89	0.85

the concrete samples in the curing chamber (98% RH and 20 °C). The samples were conditioned at 105 °C for a minimum of 24 h until weight variation was less than 0.5% in measures spaced 1 h and dry weight was measured at 20 °C. Then, the samples were immersed in water and weight was measured after 48 h and cycles of 24 h up to weight difference was less than 0.5% in consecutive measurements, eliminating the surface water of the samples. After the immersion, the samples were saturated under vacuum, applying vacuum for 2 h and then adding demineralized water slowly. When the samples were completely covered, the vacuum was removed and samples were kept in water for 24 h. The weight was measured eliminating the water in the surface. Finally, apparent weight was measured using a hydrostatic scale. The calculated porosity and saturated density are shown in Table 3.

The ponding test for the two concrete mixes was conducted according to EN 12390-11[48] but with a salt (NaCl) concentration of 165 g L^{-1} of solution as defined in NT Build 443.[42] The chloride profiles were obtained after 46 days of exposure.

4.4. Isothermal Calorimetry and In Situ XRD Analysis

To investigate the compatibility of the LDH in a high alkaline cement paste system, additional analyses were performed. They consisted of isothermal calorimetry and XRD studies on cement pastes containing two amounts of LDH. For this, cement paste samples (CEM I 42.5 LA SR) were prepared (w/c = 0.5) without, with 2 and 4 mass% LDH (calculated on the dry cement mass). This cement was chosen to better ascertain the interaction of LDH with cement. The XRD measurements (Rigaku MiniFlex 600, Cu X-ray tube at 2° min^{-1}, detected with a high-speed silicon strip detector) were performed on the hydrating cement pastes in situ over a 56 d period. The samples were casted into the XRD sample holder, covered by a Kapton film, and then periodically measured by XRD. When not measured, samples covered by the Kapton film were stored in a desiccator. Isothermal calorimetry (TamAir isothermal calorimeter) was done with in situ paste samples from 1 min to over 7 days of hydration. The samples were externally mixed in the sample vial and placed in the calorimeter.

5. Results and Discussion

5.1. Model Validation Using Accelerated Ponding Tests

The aforementioned finite element-based numerical model was used to predict the 46 day chloride profiles for both REF and +2% LDH mixes. The initial concentrations for each mix were taken from Table 4 and diffusion coefficients at infinite dilution for each species were taken from Table 2. The used Freundlich isotherm parameters are shown in Table 5. Likewise formation factor and other parameters were included from Table 3. The simulation results were compared with experimentally measured chloride profile at 46 days obtained from ponding tests.

Figure 3a shows the experimentally determined Freundlich-type chloride binding isotherm from cement paste for the REF mix. A comparison of model-predicted chloride profiles after 46 days with experimentally determined chloride profiles is shown in Figure 3b. Out of the three experimentally measured chloride profiles for REF mix, only two profiles (S1-REF and S2-REF) are considered here because one chloride profile (S3-REF, not shown here) had missing points and unusually high scatter. As shown in Figure 3b, the model does not seem to capture the first few millimeters of the chloride profile, especially the occurrence of sharp peak (skin effect) in the first few millimeters. Other physical phenomena apart from diffusion could be predominant in this region. A comparatively better prediction is observed toward deeper depths of the penetration profile with lower concentrations of Cl in the concrete. Figure 3c shows a comparison of the averaged experimental profile and modeled profile and also confirms the same conclusion.

To computationally measure the effect of Mg–Al–NO$_2$ in concrete, a similar simulation was carried for +2% LDH mix. **Figure 4**a shows the experimentally determined Freundlich-type chloride binding isotherm from cement paste for the +2% LDH mix. Figure 4b shows a comparison of 46 day model predicted chloride profile with experimentally determined chloride profile for each sample. A better agreement is observed between the modeled and experimental chloride profiles in concrete with LDH. The accuracy of the model in comparison with experiments is shown in Figure 4b. The modeled chloride front passes through the experimental scatter in the first few centimeters along the penetration path and merges very well with the experimental points along higher penetration depth of chloride front. Furthermore, S1-2% LDH and S2-2% LDH show a predominant peak in the first few millimeters, whereas the peak is less predominant in S3-2% LDH sample. As was the case with REF mix, the model does not capture the peaks in the chloride profiles but fits well beyond the first few millimeters. In general, a better fit is observed which can be appreciated from the comparison of averaged experimental profiles and modeled chloride profile as shown in Figure 4c.

In all the computations presented so far, the model is able to predict the chloride profile for a particular concrete mix with reasonable accuracy. This is primarily due to the benefit of using the formation factor, which accurately characterizes the microstructure, thereby yielding a good estimate of effective diffusion coefficient for chloride ions. Deviations in predictions especially in the first few millimeters along the penetration path can be attributed to many factors: first, the occurrence of skin effect[49–51] causes a sharp chloride peak in the first few millimeters; second, the model is sensitive to the variability in the chloride binding isotherm and also the fact that formation factor was measured at 28 d age, whereas the chloride profiles were measured after 46 days of exposure time.
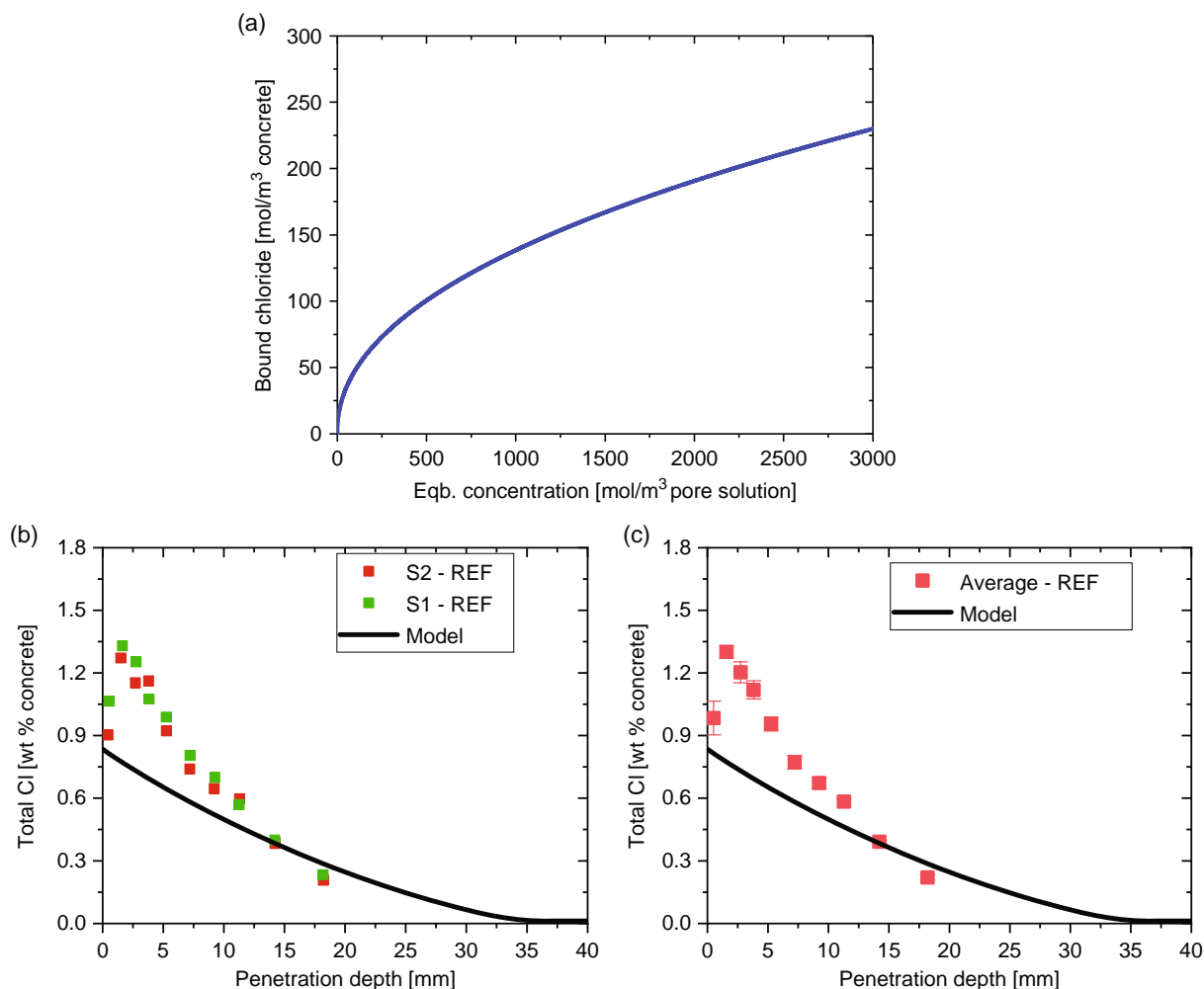
2000398 (7 of 13)

**ADVANCED
SCIENCE NEWS**
www.advancedsciencenews.com

**ADVANCED
ENGINEERING
MATERIALS**
www.aem-journal.com

Figure 3. a) Chloride binding isotherm for cement paste from REF mix. b) A comparison of predicted 46 day chloride profiles with experiments from concrete with REF mix. Prefixes S1, S2, and S3 represent the chloride profile for each sample from the ponding test. c) A comparison of predicted profile and averaged experimental profiles.

The authors recommended that both chloride profile and formation factor should be measured at the same age to have a better numerical prediction of chloride profiles. The error of prediction for both the sets is shown in **Figure 5**. The strong influence of skin effect in the first few millimeters is represented by the high error of prediction in this region. It is also observed that the error of prediction decreases along the penetration path.

5.2. Mg–Al–NO₂ Efficiency toward Additional Chloride Binding

One of the most important properties of LDHs in corrosion control is its ability to capture negatively charged ions, e.g., Cl^- from the environment together with the possibility to deliver a corrosion inhibitor such as NO_2^- via the ion exchange process. Our previous investigations have revealed that LDH can significantly decrease chloride concentrations in the surrounding environments. However, the capacity to capture chloride ions can be influenced by the amount of LDH itself as well as pH

of the surrounding environment.[52] The chloride capture is very fast and a thermodynamic heterogeneous equilibrium is established almost instantly.

The modeled profile for +2% LDH mix is slightly below the REF mix as shown in **Figure 6**a, suggesting only a moderate chloride capture in +2% LDH compared with REF mix. Similarly in Figure 6b, a comparison of experimental obtained averaged chloride profile shows only a moderate difference, with the +2% LDH profile slightly under the REF mix. The chloride binding isotherms as well show only slight differences between the two mixes as shown in Figure 6c.

This suggests that a major gain in chloride binding capacity of LDH could not be achieved. Many factors can contribute to this effect. First, a major contributing factor could be that LDH conducts a preferential exchange of NO_2^- with OH^- instead of Cl^-. This can also be observed from the pore solution analysis where high concentrations of NO_2^- was observed despite no exposure to chloride (Table 4). This implies that either LDH conducted exchange with OH^-/other ions in the pore solution or lost its

**ADVANCED
SCIENCE NEWS**
www.advancedsciencenews.com

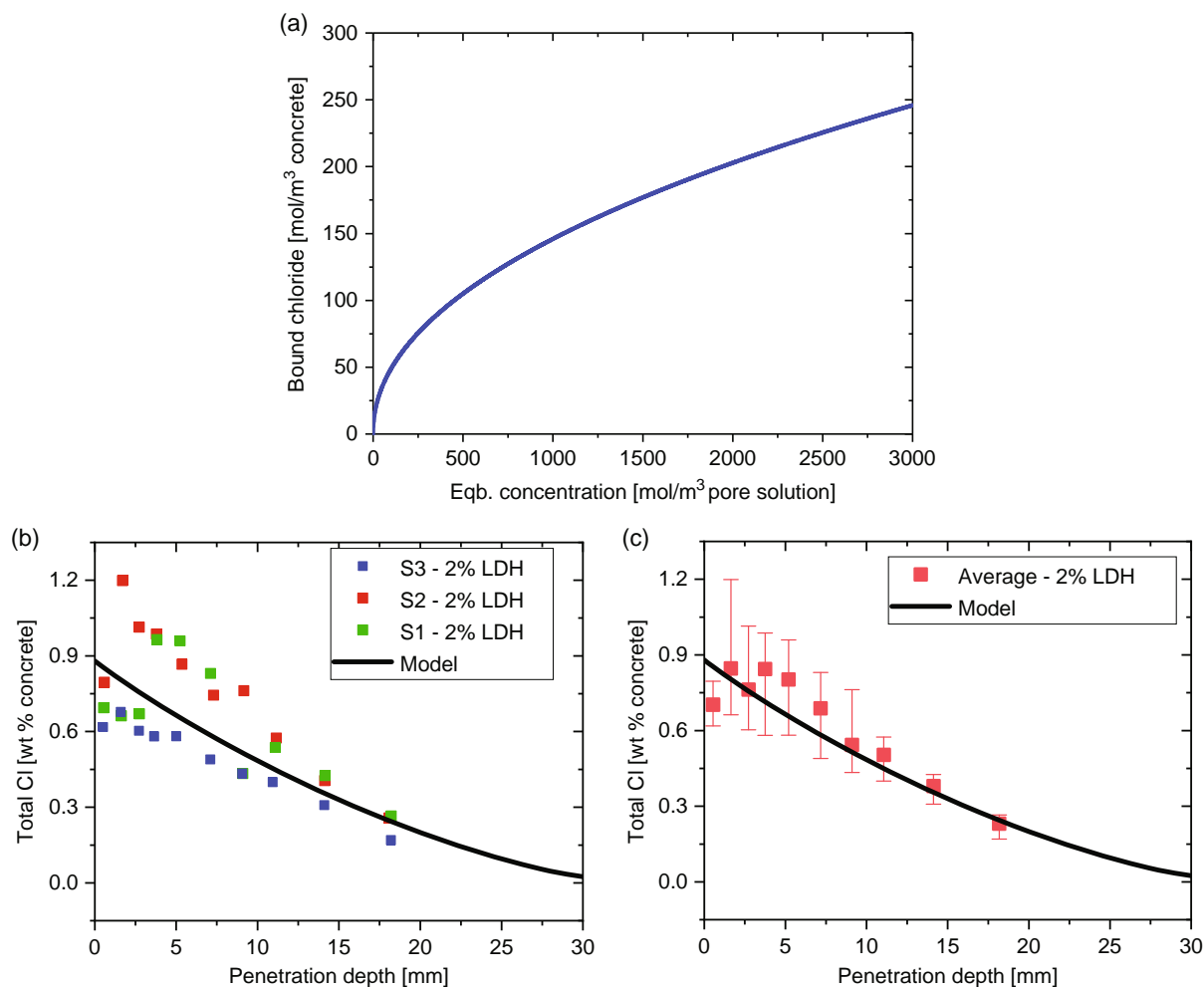**ADVANCED
ENGINEERING
MATERIALS**
www.aem-journal.com

Figure 4. a) Chloride binding isotherm for +2% LDH mix. b) A comparison of predicted 46 day chloride front compared with experiments. Prefixes S1, S2, and S3 represent the chloride profile for each sample from the ponding tests. c) A comparison of predicted profile and averaged experimental profiles.
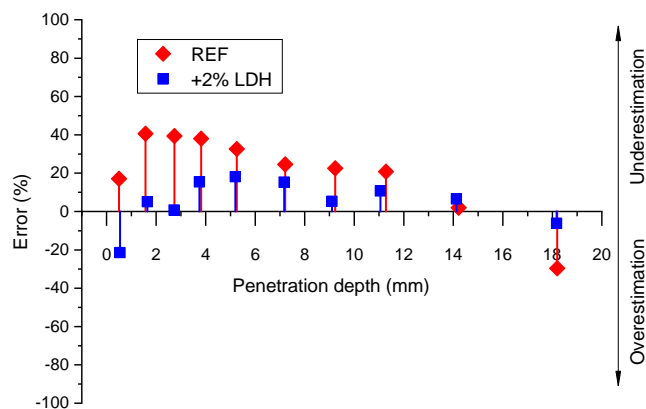

Figure 5. Error between simulation-assisted and experimentally obtained profiles for REF and +2% LDH mix.

structural stability at high alkaline pH. To confirm the release of NO_2^- in pore solution, additional pore solutions from cement paste with varying w/c ratios were analyzed (Appendix). In all the samples with LDH, the presence of NO_2^- was found in the pore solution. Second, the overall percentage of the LDH in concrete is only 2% of the binder, which is overall a very small percentage. Third, LDH could also undergo a slight dissolution at high alkaline pH ranges as mentioned previously. All these factors can potentially act together but in different proportions. To better understand the stability of LDH in cementitious environments, additional stability tests were conducted and are explained in the next section.

5.3. Stability Analysis of Mg–Al–NO₂ in Cementitious Systems

The heat flow and total heat release curves from isothermal calorimetry are shown in **Figure 7**. Heat flow curves for pastes with LDH-NO₂ showed a strong acceleration of the hydration reaction. More LDH-NO₂ seems to increase the acceleration. The earlier onset of the induction and acceleration period shifted the peak heat release from 11.4 to 10.2 h and 9.1 h, respectively. The sulfate depletion shoulder of CEM I at ≈18 h appeared earlier and moved back into the main peak
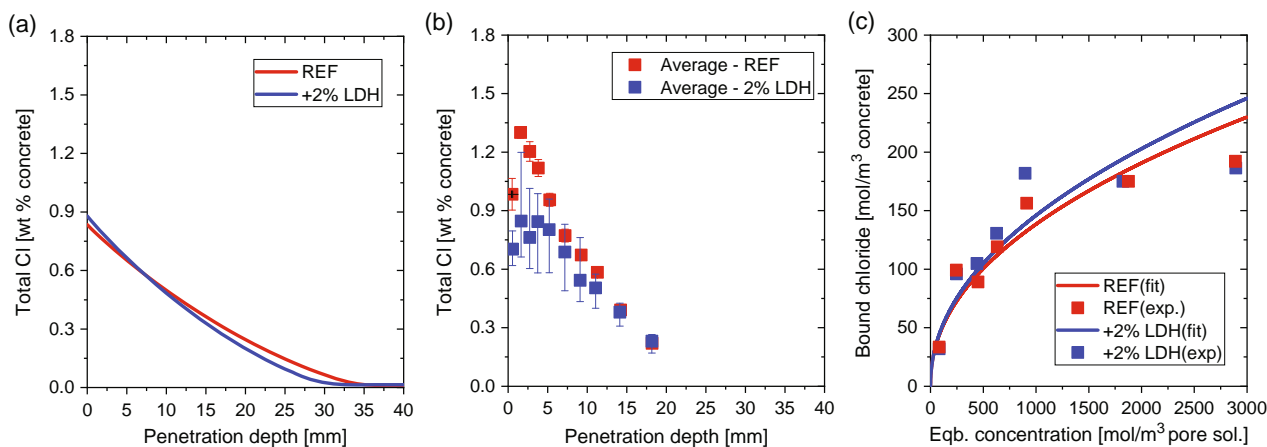
Figure 6. a) Model-predicted chloride profiles for REF and 2% Mix. b) Experimentally obtained chloride profiles including scatter for measurements. c) Experimentally obtained chloride binding isotherms and fitted Freundlich isotherms.
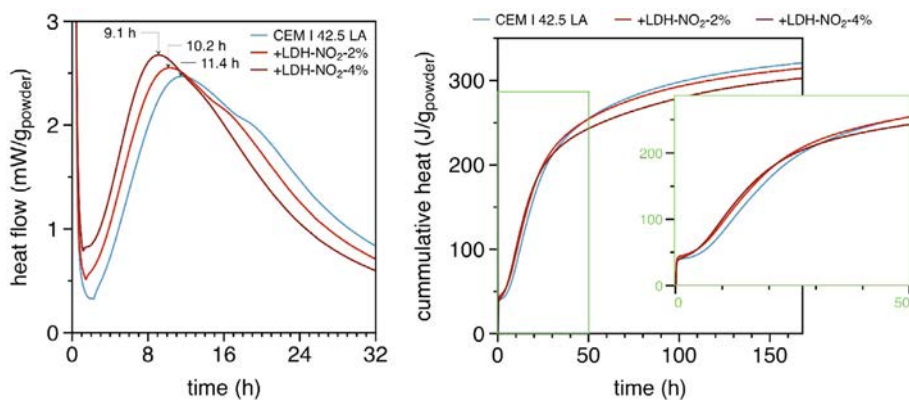

Figure 7. Heat flow curves of cement paste without and with two concentrations of LDH.

with increasing LDH content. Other authors attribute this shoulder with the formation of AFm.[53] Cumulative heat curves of LDH-NO$_2$ pastes had higher heat production between 30 (4%) and 45 h (2%) of hydration. The total heat release in this range was higher with the increase in LDH in the pastes compared with the paste with CEM I only. Afterward, the curves converged to similar values but slightly below the curve of the pure CEM I paste.

The results from XRD measurements are shown in **Figure 8**. The CEM I paste showed in all ages a moderate amount of ettringite. From 7 days appeared an ettringite double peak at 8.5° 2-theta. Some artifact peaks between 13° and 15° 2-theta appear in the 4, 7, 14, 28, 40 days measurements, probably caused due to interference with the sample holder. Even after 56 days of hydration, only minor amounts of AFm phases in the form of hemi- and monocarbonate were visible. This was due to a very low C$_3$A content of the CEM I, which was a sulfate-resistant cement.

In pastes containing CEM I + LDH-NO$_2$ moderate amounts of ettringite were visible. In pastes with 4% LDH-NO$_2$ hemi- and monocarbonate was formed after 2 d of hydration; in pastes with 2% LDH, both AFm phases appeared later.

A monosulfate peak (9.9° 2-theta) was faintly visible in some of the hydration ages. A peak between hemi- and monocarbonate was either identified as a hydrotalcite-type phase or rests of LDH-NO$_2$ (main base peak 11.36° 2-theta).

There is strong evidence from the heat flow/total heat curves and from phase developments that the LDH reacts to a certain degree within the first hours of hydration. No LDH peaks can be found even at 4% in early hydration ages. The formation of AFm phases and possibly a hydrotalcite-like phase hints at a dissolution of the Mg–Al–NO$_2$ LDH. Acceleration of the hydration in isothermal calorimetry indicates substantial reaction of LDH. A filler effect is less probable because the induction/acceleration periods and sulfate depletion/AFm formation shoulder are shifted significantly toward earlier times, which indicates a chemical reaction of the LDH and a change in nucleation kinetics of C–S–H, initiated by LDH.

The results do not clearly indicate how much of the LDH reacted and the underlying mechanism, but due to the results of the calorimetry and the amounts of formed AFm phases, it is assumed that a substantial amount of the finer particles might have reacted. Any effects of LDH in cement pastes
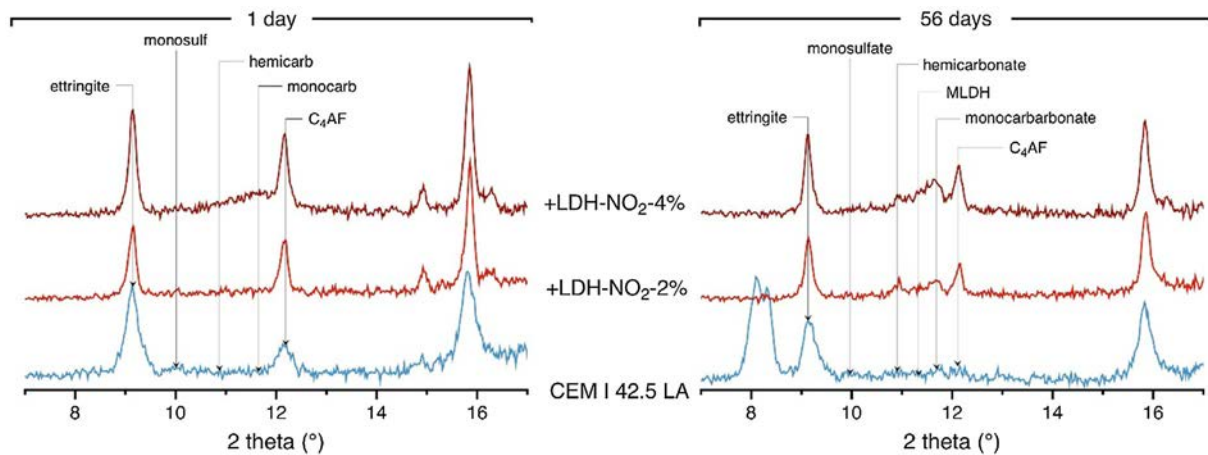
**ADVANCED
SCIENCE NEWS**
www.advancedsciencenews.com

**ADVANCED
ENGINEERING
MATERIALS**
www.aem-journal.com

Figure 8. XRD pattern of CEM I pastes without and with LDH after 1 and 56 days of hydration.

toward chloride solutions might therefore also be due to chemical binding of chloride by AFm phases rather than with LDH.

6. Conclusions

The formation factor is a material property of porous media and can be easily determined by electrical measurements.[28,36,43] Formation factor is accurately able to measure the hindrance offered by the porous microstructure on the ionic transport without taking chloride binding into account.[29] Effective diffusion coefficients obtained as such tend to be very accurate. Thus, the experimental determination of formation factor by electrical conductivity measurements is an efficient way to establish effective diffusion coefficients needed in chloride transport models.

Based on chloride binding and formation factor, different concrete mixes can be easily compared in terms of their durability toward chloride ingress. These inputs are cheaper and relatively fast to obtain. Determination of formation factor can be a suitable alternative for expensive and time-consuming standard laboratory diffusion tests.

Based on the 1D transport model described in the article, two concrete recipes i.e., with and without Mg–Al–NO$_2$ were compared. A comparison of model-predicted chloride and experimentally obtained chloride profiles from accelerated natural ponding tests was presented. The model is able to predict the chloride ingress profile with a reasonable accuracy. In REF mix, the model is not able to capture the chloride peak but converges well with experimental observed chloride profiles at deeper depth with lower Cl content. For +2% LDH mix, the chloride peak is not so predominant in the experiments and the model shows a better match with experimentally obtained profiles.

Based on the evaluation of model predicted and experimentally derived chloride profiles, only a moderate difference is observable between the two recipes with the +2% LDH mix showing slightly lower ingress compared with REF mix. This can be attributed to reduced functionality of LDH particles in hydrating cementitious matrix. Similar information is obtained from binding isotherms which do not show any significant

difference, indicating that both mixes show almost similar chloride uptake values.

Calorimetry measurements indicated that the addition of LDH caused a slight acceleration of the hydration process as well as formation of AFm phases and possibly a hydrotalcite-like phase hints at a dissolution of the Mg–Al–NO$_2$ LDH. The AFm phases generated could in turn bind chloride ions from the pore solutions.

Based on in situ XRD analysis, LDH particles in cement pastes were not observed even at 4% dosage. The authors believe that this could be in part due to LDH undergoing partial dissolution followed by subsequent reactions leading to AFm formation and in part to the small quantity of LDH, which if not dissolved is too less in quantity to be detected during XRD analysis. In addition, if LDH stays undissolved, preferential exchange with OH$^-$ instead of Cl$^-$ together with moderate dissolution of LDH at high alkaline pH can also be contributing factors toward reduced chloride capture. The authors recommended that in future additional studies must be conducted to specifically determine the exact LDH dissolution/reaction mechanism in cement paste.

Appendix

Pore solution analysis of cement paste without (REF) and with 2% Mg–Al–NO$_2$ (+2% LDH) with varying w/c ratios: Concentrations of ions are in ppm (Table A1).

Calculation of bound chloride:

The bound chloride is calculated for each sample as

$$C_{C\ell^-}^b = \left(\frac{\left(C_{C\ell^-}^o - C_{C\ell^-}^{Eq.} \right) \cdot V_{sol.}}{M_s} \right) \tag{13}$$

where $C_{C\ell^-}^o$ is the initial chloride concentration, $C_{C\ell^-}^{Eq.}$ is the final equilibrium chloride concentration after 7 days of exposure, $V_{sol.}$ is volume of the solution (50 mL), and M_s and is the mass of ground cement paste powder (10 g).

**ADVANCED
SCIENCE NEWS**

www.advancedsciencenews.com

**ADVANCED
ENGINEERING
MATERIALS**

www.aem-journal.com

Table A1. Pore solution analysis of cement pastes with different w/c.

Series-ID-(w/c)	Al^{3+}	Ca^{2+}	Mg^{2+}	K^+	Na^+	Cl^-	NO_2^-	NO_3^-	SO_4^{2-}	pH
REF-1-(0.5)	0.46	20.10	–	1709.13	938.41	74.86	–	–	53.07	13.24
REF-2-(0.5)	0.48	20.06	–	2350.86	1073.72	104.67	–	–	56.33	13.28
REF-1-(0.55)	1.35	21.75	–	14846.2	5248.74	73.92	–	–	136.12	13.40
REF-2-(0.55)	1.05	35.41	–	10841.6	3264.13	313.91	–	–	269.60	13.42
REF-1-(0.6)	1.10	11.94	–	11374.5	3469.85	64.06	–	–	131.31	13.47
REF-2-(0.6)	1.17	21.63	–	10113.6	2991.01	–	–	–	–	13.44
+2% LDH-1-(0.5)	0.43	45.50	–	2230.53	1193.68	42.46	887.28	72.31	49.94	13.27
+2% LDH-2-(0.5)	0.49	44.34	–	2166.44	1184.05	49.03	963.97	76.37	47.61	13.25
+2% LDH-1-(0.55)	1.42	32.64	–	11360.2	4511.28	58.93	1994.54	105.78	144.71	13.38
+2% LDH-2-(0.55)	1.25	41.38	–	11682.1	4482.01	80.19	1923.89	110.97	123.93	13.40
+2% LDH-1-(0.6)	1.30	7.30	–	12125.6	4613.18	161.60	2018.66	104.89	199.98	13.38
+2% LDH-2-(0.6)	0.94	7.83	–	9944.91	3638.54	37.36	1409.18	46.82	109.40	13.38

Conflict of Interest

The authors declare no conflict of interest.

Author Contributions

Conceptualization: Z.M., A.C.B., C.G., and L.D.H. Synthesis: F.R. and C.R. Finite element model: Z.M. and P.M. Experiments: U.M., M.C., K.V., M.P., C.G., and A.C.B. Analysis of results and data treatment: Z.M., U.M., A.C.B., C.G., M.C., K.V., M.P., and P.M. Manuscript writing and editing: Z.M., U.M., and A.C.B. Supervision: A.C.B., D.H., U.M., M.C., M.G.S.F., and M.L.Z.

[1] K. Tuutti, *Corrosion of Steel in Concrete: Technical Report*, Swedish Cement and Concrete Research Institute, Stockholm **1982**.

[2] B. E. L. Bertolini, P. Pedeferri, E. Redaelli, R. Polder, *Corrosion of Steel in Concrete: Prevention, Diagnosis, Repair*, Wiley-VCH, Weinheim **2013**.

[3] Z. P. Bazant, *J. Struct. Div. ASCE* **1979**, *105*, 1137.

[4] U. Angst, *Mater. Struct.* **2018**, *51*, 1.

[5] A. Poursaee, C. M. Hansson, *Cement Concrete Res.* **2007**, *37*, 1127.

[6] D. Boubitsas, T. Luping, P. Utgenannt, *Chloride Ingress in Concrete Exposed to Marine Environment – Field Data up to 20 Years' Exposure*, Swedish Cement and Concrete Research Institute (CBI), Sweden **2014**.

[7] P. Ghods, O. B. Isgor, G. J. C. Carpenter, J. Li, G. A. McRae, G. P. Gu, *Cement Concrete Res.* **2013**, *47*, 55.

[8] U. M. Angst, M. R. Geiker, A. Michel, C. Gehlen, H. Wong, O. B. Isgor, B. Elsener, C. M. Hansson, R. Francois, K. Hornbostel, R. Polder, M. C. Alonso, M. Sanchez, M. J. Correia, M. Criado, A. Sagues, N. Buenfeld, *Mater. Struct.* **2017**, *50*, 1.

[9] R. Vera, M. Villarroel, A. M. Carvajal, E. Vera, C. Ortiz, *Mater. Chem. Phys.* **2009**, *114*, 467.

[10] F. J. Molina, C. Alonso, C. Andrade, *Mater. Struct.* **1993**, *26*, 532.

[11] C. Andrade, C. Alonso, F. J. Molina, *Mater. Struct.* **1993**, *26162*, 453.

[12] E. Sola, Ph.D. Thesis, Institute of Construction Materials, University of Stuttgart **2017**.

[13] E. Sola, J. Ozbolt, G. Balabanic, Z. M. Mir, *Cement Concrete Res.* **2019**, *120*, 119.

[14] Q. Yuan, C. J. Shi, G. De Schutter, K. Audenaert, D. H. Deng, *Constr. Build. Mater.* **2009**, *23*, 1.

[15] I. G. Richardson, *Cement Concrete Comp.* **2000**, *22*, 97.

[16] H. Justnes, *Nordic Concrete Res.*, **1998**, *21*, 48.

[17] B. Martin-Perez, H. Zibara, R. D. Hooton, M. D. A. Thomas, *Cement Concrete Res.* **2000**, *30*, 1215.

[18] H. Zibara, *Binding of External Chlorides by Cement Pastes*, University of Toronto, Toronto, Canada **2001**.

[19] European Union's Project, *Lorcenis – Long Lasting Reinforced Concrete for Energy Infrastructure Under Severe Operating Conditions*, SINTEF, Norway **2016–2020**.

[20] E. L. Crepaldi, P. C. Pavan, J. B. Valim, *J. Brazil. Chem. Soc.* **2000**, *11*, 64.

[21] J. Tedim, A. Kuznetsova, A. N. Salak, F. Montemor, D. Snihirova, M. Pilz, M. L. Zheludkevich, M. G. S. Ferreira, *Corros. Sci.* **2012**, *55*, 1.

[22] M. Meyn, K. Beneke, G. Lagaly, *Inorg. Chem.* **1990**, *29*, 5201.

[23] Y. H. Cao, D. J. Zheng, S. G. Dong, F. Zhang, J. Y. Lin, J. Wang, C. J. Lin, *J. Electrochem. Soc.* **2019**, *166*, C3106.

[24] J. D. Zuo, B. Wu, C. Y. Luo, B. Q. Dong, F. Xing, *Corros. Sci.* **2019**, *152*, 120.

[25] Z. Yang, R. Polder, J. Mol, C. Andrade, *Cement Concrete Res.* **2017**, *100*, 186.

[26] Z. X. Yang, H. Fischer, R. Polder, *Cement Concrete Comp.* **2014**, *47*, 87.

[27] Y. Y. Wu, P. Duan, C. J. Yan, *Appl. Clay Sci.* **2018**, *158*, 123.

[28] W. J. Weiss, T. J. Barrett, C. Qiao, H. Todak, *Adv. Civ. Eng. Mater.* **2016**, *5*, 179.

[29] K. A. Snyder, *Concr. Sci. Eng.* **2001**, *3*, 216.

[30] L. P. Tang, L. O. Nilsson, *Cement Concrete Res.* **1993**, *23*, 247.

ADVANCED
SCIENCE NEWS

www.advancedsciencenews.com

ADVANCED
ENGINEERING
MATERIALS

www.aem-journal.com

[31] C. Y. Qiao, A. T. Coyle, O. B. Isgor, W. J. Weiss, *Adv. Civ. Eng. Mater.* **2018**, *7*, 206.

[32] K. Karadakis, V. J. Azad, P. Ghods, O. B. Isgor, *J. Electrochem. Soc.* **2016**, *163*, C306.

[33] T. Belytschko, W. K. Liu, B. Moran, K. I. Elkhodary, *Nonlinear Finite Elements for Continua and Structures*, Wiley, Chichester, West Sussex **2014**.

[34] S. K. Poznyak, J. Tedim, L. M. Rodrigues, A. N. Salak, M. L. Zheludkevich, L. F. P. Dick, M. G. S. Ferreira, *ACS Appl. Mater. Inter.* **2009**, *1*, 2353.

[35] P. Spiesz, H. J. H. Brouwers, *Cement Concrete Res.* **2013**, *48*, 116.

[36] G. E. Archie, *Trans. AIME* **1942**, *146*, 54.

[37] D. Hoche, *J. Electrochem. Soc.* **2015**, *162*, C1.

[38] T. Luping, L.-O. Nilsson, *Cement Concrete Res.* **1993**, *23*, 247.

[39] E. Samson, J. Marchand, *J. Colloid Interface Sci.* **1999**, *215*, 1.

[40] Q. F. Liu, D. Easterbrook, J. Yang, L. Y. Li, *Eng. Struct.* **2015**, *86*, 122.

[41] E. Samson, J. Marchand, *Cement Concrete Res.* **2007**, *37*, 455.

[42] NT BUILD 443, *Concrete, Hardened: Accelerated Chloride Penetration, Nord Test Method*, Nordtest, Finland **1995**.

[43] Pwi pren 12390-xz Determination of Electrical Resistivity-updated 2020-Feb Draft Version, European Standard – Technical Committee CEN/TC 104 – Secretariat: DIN.

[44] M. C. Alonso, J. L. García Calvo, S. Pettersson, I. Puigdomenech, M. A. Cuñado, M. Vuorio, H. Weber, H. Ueda, M. Naito, C. Walker, Y. Takeshi, C. Cau-Dit-Coumes, in *Cement-Based Materials for Nuclear Waste Storage*, Springer, New York, NY **2012** pp. 251–259.

[45] A. Delagrave, J. Marchand, J. P. Ollivier, S. Julien, K. Hazrati, *Adv. Cement Base. Mater.* **1997**, *6*, 28.

[46] C. Y. Qiao, W. Ni, Q. H. Wang, J. Weiss, *J. Mater. Civil Eng.* **2018**, *30*.

[47] UNE 83980 : 2014 – Concrete Durability. Test Methods. Determination of the Water Absorption, Density and Accessible Porosity for Water in Concrete. Spanish Association for Standardization and Certification, **2014**, https://www.une.org/encuentra-tu-norma/busca-tu-norma/norma/?c=N0054056.

[48] BSI, EN 12390-11:2015 – Testing Hardened Concrete. Determination of the Chloride Resistance of Concrete, Unidirectional Diffusion, **2015**, https://shop.bsigroup.com/ProductDetail?pid=000000000030351885.

[49] C. Andrade, L. M. Diez, C. Alonso, *Adv. Cement Base. Mater.* **1997**, *6*, 39.

[50] P. Castro, O. T. De Rincon, E. Pazini, *Cement Concrete Res.* **2001**, *31*, 529.

[51] K. De Weerdt, D. Orsáková, A. C. Müller, C. K. Larsen, B. Pedersen, M. R. Geiker, *Constr. Build. Mater.* **2016**, *120*, 418.

[52] C. Gomes, Z. Mir, R. Sampaio, A. Bastos, J. Tedim, F. Maia, C. Rocha, M.G.S. Ferriera, *Materials* **2020**, *13*, 1769.

[53] A. Fernandez, M. C. Alonso, J. L. Garcia-Calvo, B. Lothenbach, *Mater. Construct.* **2016**, *66*, 1.

[54] K. Karadakis, *Numerical Investigation of the Chemistry of the Pore Solution in the Mill Scale Crevices of Carbon Steel Rebar*, Vol. Master of Applied Science, Department of Civil and Environmental Engineering, Carleton University, Ottawa, ON, Canada **2010**.